Coupled Systems Mechanics, *Vol. 15, No. 3 (2026) 211-226*
https://doi.org/10.12989/csm.2026.15.3.211

Techno-Press

Comparison study for thermal buckling behavior of laminated shallow shell

Ibtehal A. Sadiq[a], Widad I. Majeed*

Department of Mechanical Engineering, College of Engineering, University of Baghdad, Baghdad, Republic of Iraq

(Received November 13, 2025, Revised March 31, 2026, Accepted May 27, 2026)

Abstract. Thermal buckling analysis of laminated shallow spherical shell using two higher order theories for first time, based on (Mantari displacement field) and (Reddy displacement field) are developed. The equations of motion are derived using Hamilton' s principle and solved using Navier-type for simply supported boundary conditions. The effect of various design parameters such as thickness ratio, orthotropy ratio, shallowness ratio and number of layer for laminated shell have been studied also compared with other published results which give good agreement and have same behavior when changing design parameters, and they are closed to each other except that thermal buckling mode sometimes changed.

Keywords: composite material; high shear deformation theory; shells; stability; thermal buckling

1. Introduction

Many engineering applications of composite plates and shells are used in aerospace, automobiles, civil engineering which is always under complicated loads such as thermal loading due to the aerodynamic heating during their service life. Buckling in the structure is caused by increasing temperature which affects the performance of structure. Thermal buckling was important to predict the predominant cause of failure of laminated composite shells subjected to severe thermal loadings. Many researchers investigated thermal buckling of laminated beam, plates and shell, for example, [1] used Timoshenko beam theory and Lagrangian approach to investigate thermal buckling and post-buckling phenomena occurs with immovable ends of the beam also [2] studied thermal buckling and post-buckling behaviors of functionally graded materials (FGM) tubes subjected to a uniform temperature rise and resting on elastic foundations using a refined beam model. [3] used three-dimensional solutions to obtain critical temperature of laminated plates but [4, 5, 6] developed new displacement function for thermal buckling of laminated plates, also [7], investigated thermal bucking analysis for cross ply laminated plates using different theories while [8], analyzed stress of a laminated simply supported plate with porosity under hygro thermal rising using first shear plate deformation theory.

Many other researchers [9, 10, 11] developed four and five variable refined plate theory to

*Corresponding author, Professor, E-mail: wedad.ibrahim@coeng.uobaghdad.edu.iq
[a] Professor

http://www.techno-press.org/csm/5
ISSN: 2234-2184 (Print), 2234-2192 (Online)

solve buckling equations of motion for composite plates under thermal environment. Also [12, 13] studied thermal buckling of laminated plates under thermal and mechanical loading while [14], analyzed critical buckling temperature response of FGP sandwich plates under various boundary conditions. But [15] investigated wave propagation analysis of functionally graded sandwich plate with different porosity distributions in thermal environment also [16] studied thermal buckling of laminated composite plates using finite element method for different boundary conditions, while [17] used commercial software ABAQUS to predict the critical buckling temperature of the Bouligand inspired laminated plates under thermal loading concluding that as the pitch angle is increased, mechanical and thermal properties chieved by the Bouligand structure of laminates can be improved. Researcher [18] studied the thermal buckling of ceramic-metal FG sandwich plates with a homogeneous core and two FGM face sheets. The mathematical model formulated according to 3-D thermo-elasticity and approximated by making use of a hierarchical model and 2-D natural element method (NEM), also [19] analyzed thermal buckling and postbuckling behavior of a functionally graded (FG) graphene platelet-reinforced composite plate using finite element method based on first order shear deformation theory.

Sets of algebraic equation are obtained using suitable finite element, such as [20] investigated thermal post buckling behavior under uniform and non-uniform temperature distribution using finite element method of batched laminated panels while [21], developed nonlinear finite element model to find thermal post-buckling of laminated composite cylindrical/hyperboloid shell panel uniform temperature field used direct iterative approach. Researcher [22], investigated vibration and thermal buckling characteristics of Spherical, cylindrical, hyperboloid and elliptical shells using higher order shear deformation theory for curved laminated composite structures also [23] studied thermoelastic buckling composite spherical and cylindrical shells under non-uniform and uniform thermal fields using finite element methods and higher-order theory. Researchers [24] studied buckling and post-buckling behavior of the FG structures under uniform and nonuniform temperature distributions using large displacements and finite rotation to accurately model and [25] developed a new numerical method hierarchical model and 2-D natural element method (NEM) to study thermal buckling of metal-ceramic functionally graded (FG) plates, while [26], evaluated post-buckling strength of the tilted sandwich composite shell structure using nonlinear finite element model also [27], focused on how structure behave under thermal loads as the temperature of the structure increase showing its effect on the natural frequency and thermal buckling load using Carrera Unified Formulation (CUF) while [28] developed finite element type higher-order formulation to analyze thermal eigenvalue of the graded sandwich shell structure under variable thermal loadings. Researcher [29] developed higher order shear deformation theory to fined critical temperatures of cross-ply shallow shells using power series method also [30] used first-order shear deformation theory to study thermal buckling behavior of laminates cylindrical shells subjected to uniformly distributed temperature load. Researcher [31], developed mathematical model of laminated composite single/doubly curved (cylindrical/ spherical/ hyperboloid/ elliptical) panel using higher order shear deformation theory subjected to in-plane (thermal/mechanical/thermo-mechanical) while [32] investigated thermal buckling behavior of laminated spherical shallow shell subjected to uniform temperature distribution, governing equations are solved using Levy type method based on first-order shear deformation theory, also [33] investigated thermal buckling behavior of laminated spherical shallow shell subjected to uniform temperature distribution, using Levy type method based on higher order shear deformation shallow shell theory. Researchers [34] studied thermal buckling and post-buckling behaviors of imperfect graphene reinforced metal foams (GPRMFs) doubly curved shells.

Since some displacement field were used to analyze static and dynamic behavior of plates and shells, however some of them could not give close results for buckling or thermal buckling therefore we examine (Mantari and Reddy functions) for first time to analyze thermal buckling of shell. In present work, thermal buckling of cross ply laminated shallow spherical shells are analyzed by solving equations of motion derived based on two theories, first one is Mantari displacement field in which the displacements of the middle surface are expanded as a combination of exponential and polynomial functions of the thickness coordinate and second one is Reddy displacement fields in which the displacements of the middle surface are expanded as a polynomial functions of the thickness coordinate. Many design parameters such as (thickness, shallowness, etc.) ratio and number of layer are considered and compare with other researchers.

2. Displacement and strain

Displacements of the middle surface are expanded as a combination of exponential and polynomial functions of the thickness coordinate which is HOSDT developed by Mantari, keeping same assumptions, such as free boundary conditions at the top and bottom surfaces of the panel, the proposed displacement field in Cartesian coordinate system, is [35]:

$$\begin{gathered}\bar{u}(x_1,x_2,z)=u+\ z\left(m^{-2\left(\frac{z}{H}\right)^2}\theta_1-\frac{\partial w}{\partial x_1}\right)\\ \bar{v}(x_1,x_2,z)=v+\ z\left(m^{-2\left(\frac{z}{H}\right)^2}\theta_2-\frac{\partial w}{\partial x_2}\right)\\ \bar{w}(x_1,x_2,z)=w\end{gathered}\tag{1}$$

For m=constant≥0 and for thin shell $(\frac{z}{R_1})$<<1 and $(\frac{z}{R_2})$<<1: $1+\frac{z}{R_1}=1$ and $1+\frac{z}{R_2}=1$. The second HOSDT based on displacement field depending on polynomial functions of the thickness coordinate for composite shell proposed by [36] is:

$$\begin{gathered}\bar{u}(x_1,x_2,z)=u+z*\theta_1+z^3*\left(-\frac{4}{3*H}\right)*(\theta_1+\frac{\partial w}{\partial x_1})\\ \bar{v}(x_1,x_2,z)=v+z*\theta_2+z^3*\left(-\frac{4}{3*H}\right)*(\theta_2+\frac{\partial w}{\partial x_2})\\ \bar{w}(x_1,x_2,z)=w\end{gathered}\tag{2}$$

Where: $u, v, w, \theta_1, \theta_2$: are the five unknown functions as shown in Fig. 1. For all coming derivation will base on first HOSDT while the stiffness matrix obtained from each theory is given in appendix.

Applying strain-displacement relations [35], the resultant strain for first HOSDT, are:

$$\begin{gathered}\varepsilon_1=\varepsilon_1^0-z\varepsilon_1^1+z\times f(z)\varepsilon_1^2\\ \varepsilon_2=\varepsilon_2^0-z\varepsilon_2^1+z\times f(z)\varepsilon_2^2\\ \varepsilon_4=\varepsilon_4^3\times\left[1-4\times\left(\frac{z}{H}\right)^2 ln(m)\right]\times m^{-2\left(\frac{z}{H}\right)^2}\\ \varepsilon_5=\varepsilon_5^3\times\left[1-4\times\left(\frac{z}{H}\right)^2 ln(m)\right]\times m^{-2\left(\frac{z}{H}\right)^2}\\ \varepsilon_6=\varepsilon_6^0-z\varepsilon_6^1+z\times f(z)\varepsilon_6^2\end{gathered}\tag{3}$$

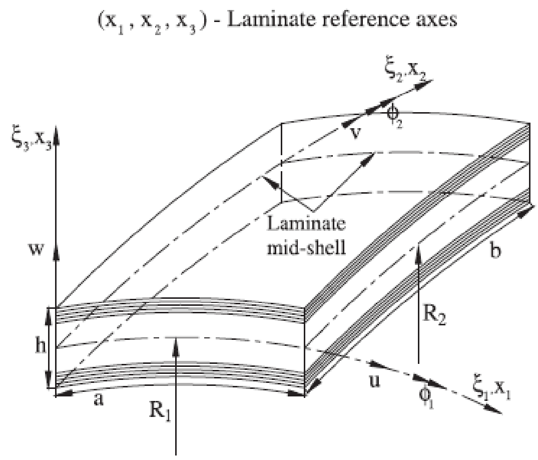

Figure 1. Shell geometry with lamination reference axes and displacement components [29]

Where:

$$f(z) = z \times \mathrm{m}^{-2\left(\frac{\mathrm{z}}{\mathrm{H}}\right)^{2}} \tag{4}$$

Strain can be written as below:

$$\begin{Bmatrix} \varepsilon_1^0 \\ \varepsilon_2^0 \\ \varepsilon_6^0 \end{Bmatrix} = \begin{Bmatrix} \frac{\partial \mathrm{u}}{\partial \mathrm{x}_1} + \frac{\mathrm{w}}{\mathrm{R}_1} \\ \frac{\partial \mathrm{v}}{\partial \mathrm{x}_2} + \frac{\mathrm{w}}{\mathrm{R}_2} \\ \frac{\partial \mathrm{v}}{\partial \mathrm{x}_1} + \frac{\partial \mathrm{u}}{\partial \mathrm{x}_2} \end{Bmatrix}, \begin{Bmatrix} \varepsilon_1^1 \\ \varepsilon_2^1 \\ \varepsilon_6^1 \end{Bmatrix} = \begin{Bmatrix} \frac{\partial^2 w}{\partial {\mathrm{x}_1}^2} \\ \frac{\partial^2 w}{\partial {\mathrm{x}_2}^2} \\ 2\frac{\partial^2 w}{\partial \mathrm{x}_1 \partial \mathrm{x}_2} \end{Bmatrix}, \begin{Bmatrix} \varepsilon_1^2 \\ \varepsilon_2^2 \\ \varepsilon_6^2 \end{Bmatrix} = \begin{Bmatrix} \frac{\partial \theta_1}{\partial \mathrm{x}_1} \\ \frac{\partial \theta_2}{\partial \mathrm{x}_2} \\ \frac{\partial \theta_2}{\partial \mathrm{x}_1} + \frac{\partial \theta_1}{\partial \mathrm{x}_2} \end{Bmatrix} \begin{Bmatrix} \varepsilon_4^3 \\ \varepsilon_5^3 \end{Bmatrix} = \begin{Bmatrix} \theta_1 \\ \theta_2 \end{Bmatrix} \tag{5}$$

3. Principle of virtual work

The equations of motion will be derived depending on first HOSDT of shells using Hamilton's principles [36].

$$0 = \int_0^t \delta U + \delta V \tag{6}$$

Where: δU is the virtual strain energy:

$$\delta\, U = \left[\int_{\frac{-h}{2}}^{\frac{h}{2}} \{\int_{\Omega}^{k} \sigma_1 \delta\, \varepsilon_1^k + \sigma_2 \delta \varepsilon_2^k + \sigma_6 \delta \varepsilon_6^k + \sigma_4 \delta \varepsilon_4^k + \sigma_5 \delta \varepsilon_5^k] \partial \mathrm{z}\, \} \partial \mathrm{x}_1 \partial \mathrm{x}_2\right] \tag{7}$$

$$\delta \mathrm{U} = \int (N_1 \delta\, \varepsilon_1^0 + M_1 \delta \varepsilon_1^1 + P_1 \delta \varepsilon_1^2 + N_2 \delta \varepsilon_2^0 + M_2 \delta \varepsilon_2^1 + P_2 \delta \varepsilon_2^2 + N_6 \delta \varepsilon_6^0 + M_6 \delta \varepsilon_6^1 + P_6 \delta \varepsilon_6^2 + K_2 \delta \varepsilon_4^3 + K_1 \delta \varepsilon_5^3)\, \partial \mathrm{x}_1 \partial \mathrm{x}_2 \tag{8}$$

Substituting Eq. (3) into Eq. (8) and integrating by parts to relative virtual displacement (δu, δv, δw, $\delta\theta_1, \delta\theta_2$), result in:

$$0=-\int[\frac{\partial N_1}{\partial x_1}\delta u+\frac{N_1}{R_1}\delta w+\frac{\partial^2 M_1}{\partial {x_1}^2}\delta w+\frac{\partial P_1}{\partial x_1}\delta\Theta_1+\frac{\partial N_2}{\partial x_2}\delta v+\frac{N_2}{R_2}\delta w-\frac{\partial^2 M_2}{\partial {x_2}^2}\delta w+\frac{\partial P_2}{\partial x_2}\delta\Theta_2+ \frac{\partial N_6}{\partial x_2}\delta u+\frac{\partial N_6}{\partial x_1}\delta v+2\frac{\partial^2 M_2}{\partial x_1\partial x_2}\delta w+\frac{\partial P_6}{\partial x_1}\delta\Theta_2+\frac{\partial P_6}{\partial x_2}\delta\Theta_1+K_1\delta\Theta_1-K_2\delta\Theta_2]\partial x_1\partial x_2 \tag{9}$$

The Virtual external work done by thermal applied load (δV) is:

$$\delta V=-\frac{1}{2}\int_0^b\int_0^a\left[N_{x1}^T\delta\left(\frac{\partial w}{\partial x_1}\right)^2+N_{x2}^T\delta\left(\frac{\partial w}{\partial x_2}\right)^2+N_{x1x2}^T\delta\left(\frac{\partial w}{\partial x_1}\frac{\partial w}{\partial x_2}\right)\right]\partial x_1\partial x_2 \tag{10}$$

Where:

$$\begin{gathered}\{N_i,M_i,P_i\}=\int_{-(\frac{h}{2})}^{(\frac{h}{2})}\sigma_i\left\{1,z,zm^{\left(-2*\left(\frac{z}{h}\right)^2\right)}\right\}dz \qquad (i=1,2,6)\\ \{K_j\}=\int_{-(\frac{h}{2})}^{(\frac{h}{2})}\sigma_i\left\{\left(1-4\log(m)\left(\frac{z}{h}\right)^2\right)m^{-2*\left(\frac{z}{h}\right)^2}\right\}dz \quad (i=4,5),\ (j=1,2)\end{gathered} \tag{11}$$

Where $\{N^T\}$ is the thermal stress:

$$\begin{Bmatrix}N_{x1}^T\\N_{x2}^T\\N_{x1x2}^T\end{Bmatrix}=\sum_{K=1}^N\int_{\frac{-h}{2}}^{\frac{h}{2}}\begin{bmatrix}\bar{Q}_{11}&\bar{Q}_{12}&\bar{Q}_{16}\\\bar{Q}_{12}&\bar{Q}_{22}&\bar{Q}_{26}\\\bar{Q}_{16}&\bar{Q}_{26}&\bar{Q}_{66}\end{bmatrix}\begin{Bmatrix}\alpha_{x1}\\\alpha_{x2}\\\alpha_{x1x2}\end{Bmatrix}\Delta Tcr\,dz \tag{12}$$

$$[A_{ij}]=\int_{\frac{-h}{2}}^{\frac{h}{2}}[\bar{Q}_{ij}]\{\alpha_{ij}\}dz\ ,\quad i,j=(1,2,6) \tag{13}$$

α_{x1},α_{x2}, and α_{x1x2} are the transformed thermal coefficients of expansion defined as:

$$\begin{gathered}\alpha_{x1}=\alpha_1(cos\,\theta)^2+\alpha_2(sin\,\theta)^2\\ \alpha_{x2}=\alpha_1(sin\,\theta)^2+\alpha_2(cos\,\theta)^2\\ 2\alpha_{x1x2}=2(\alpha_1-\alpha_2)\,sin\,\theta\,cos\,\theta\end{gathered} \tag{14}$$

Transformed plane stress stiffness terms ($[\bar{Q}_{ij}]$) are defined in [36], while α_1,α_2 are thermal expansions coefficients of longitudinal and transverse respectively, and θ is the angle of lamination. For the uniform temperature rises:

$$\Delta T=T_f-T_{ref} \tag{15}$$

Where T_f is the raised final value of temperature in which the buckling of the plate is occurring and T_{ref} is the initial temperature of plate.

4. Equations of motion

Five equations are obtained from equating terms of each virtual displacement components in Eq. (6), to zero as follows:

$$\delta u:\ \frac{\partial N_1}{\partial x_1}+\frac{\partial N_6}{\partial x_2}=0$$

$$\delta v:\ \frac{\partial N_2}{\partial x_2}+\frac{\partial N_6}{\partial x_1}=0$$

$$\delta w{:}\,2\frac{\partial^2 M_6}{\partial x_1 \partial x_2}+\frac{\partial^2 M_1}{\partial x_1^2}+\frac{\partial^2 M_2}{\partial x_2^2}-\frac{N_1}{R_1}-\frac{N_2}{R_2}+\left(N_{x1}^T\,\frac{\partial^2(w_b+w_s)}{\partial x_1^2}+N_{x2}^T\,\frac{\partial^2(w_b+w_s)}{\partial x_2^2}+2N_{x1x2}^T\,\frac{\partial^2(w_b+w_s)}{\partial x_1 \partial x_2}\right)=0$$

$$\delta\Theta_1{:}\ \frac{\partial P_1}{\partial x_1}+\frac{\partial P_6}{\partial x_2}-K_1=0 \tag{16}$$

$$\delta\Theta_2{:}\ \frac{\partial P_2}{\partial x_2}+\frac{\partial P_6}{\partial x_1}-K_2=0$$

The result forces are given by:

$$\begin{Bmatrix}N_1\\N_2\\N_6\end{Bmatrix}=\sum_{k=1}^{N}\int_{z^k}^{z^{k+1}}\begin{Bmatrix}\sigma_1\\\sigma_2\\\sigma_6\end{Bmatrix}dz$$

$$\begin{Bmatrix}M_1\\M_2\\M_6\end{Bmatrix}=\sum_{k=1}^{N}\int_{z^k}^{z^{k+1}}\begin{Bmatrix}\sigma_1\\\sigma_2\\\sigma_6\end{Bmatrix}z\,dz\ ,\ \begin{Bmatrix}P_1\\P_2\\P_6\end{Bmatrix}=\sum_{k=1}^{N}\int_{z^k}^{z^{k+1}}\begin{Bmatrix}\sigma_1\\\sigma_2\\\sigma_6\end{Bmatrix}f(z)\,dz \tag{17}$$

$$\begin{Bmatrix}K_1\\K_2\end{Bmatrix}=\sum_{k=1}^{n}\begin{Bmatrix}\sigma_5\\\sigma_4\end{Bmatrix}f(z)\partial z$$

The transformed stress-strain relation of an orthotropic lamina in a plane stress is:

$$\begin{Bmatrix}\sigma_1\\\sigma_2\\\sigma_6\end{Bmatrix}=\begin{bmatrix}Q_{11}Q_{12}Q_{16}\\Q_{12}Q_{22}Q_{26}\\Q_{16}Q_{26}Q_{66}\end{bmatrix}\begin{Bmatrix}\varepsilon_1\\\varepsilon_2\\\varepsilon_6\end{Bmatrix}\ ,\ \begin{Bmatrix}\sigma_4\\\sigma_5\end{Bmatrix}=\begin{bmatrix}Q_{44}&Q_{45}\\Q_{45}&Q_{55}\end{bmatrix}\begin{Bmatrix}\varepsilon_4\\\varepsilon_5\end{Bmatrix} \tag{18}$$

Substituting Eq. (18) in Eq. (17), and integrate them result in:

$$\begin{Bmatrix}N_1\\N_2\\N_6\end{Bmatrix}=\begin{bmatrix}A_{11}A_{12}A_{16}\\A_{12}A_{22}A_{26}\\A_{16}A_{26}A_{66}\end{bmatrix}\begin{Bmatrix}\varepsilon_1^0\\\varepsilon_2^0\\\varepsilon_6^0\end{Bmatrix}+\begin{bmatrix}B_{11}B_{12}B_{16}\\B_{12}B_{22}B_{26}\\B_{16}B_{26}B_{66}\end{bmatrix}\begin{Bmatrix}\varepsilon_1^1\\\varepsilon_2^1\\\varepsilon_6^1\end{Bmatrix}+\begin{bmatrix}E_{11}E_{12}E_{16}\\E_{12}E_{22}E_{26}\\E_{16}E_{26}E_{66}\end{bmatrix}\begin{Bmatrix}\varepsilon_1^2\\\varepsilon_2^2\\\varepsilon_6^2\end{Bmatrix} \tag{19}$$

$$\begin{Bmatrix}M_1\\M_2\\M_6\end{Bmatrix}=\begin{bmatrix}B_{11}B_{12}B_{16}\\B_{12}B_{22}B_{26}\\B_{16}B_{26}B_{66}\end{bmatrix}\begin{Bmatrix}\varepsilon_1^0\\\varepsilon_2^0\\\varepsilon_6^0\end{Bmatrix}+\begin{bmatrix}D_{11}D_{12}D_{16}\\D_{12}D_{22}D_{26}\\D_{16}D_{26}D_{66}\end{bmatrix}\begin{Bmatrix}\varepsilon_1^1\\\varepsilon_2^1\\\varepsilon_6^1\end{Bmatrix}+\begin{bmatrix}F_{11}F_{12}F_{16}\\F_{12}F_{22}F_{26}\\F_{16}F_{26}F_{66}\end{bmatrix}\begin{Bmatrix}\varepsilon_1^2\\\varepsilon_2^2\\\varepsilon_6^2\end{Bmatrix} \tag{20}$$

$$\begin{Bmatrix}P_1\\P_2\\P_6\end{Bmatrix}=\begin{bmatrix}E_{11}E_{12}E_{16}\\E_{12}E_{22}E_{26}\\E_{16}E_{26}E_{66}\end{bmatrix}\begin{Bmatrix}\varepsilon_1^0\\\varepsilon_2^0\\\varepsilon_6^0\end{Bmatrix}+\begin{bmatrix}F_{11}F_{12}F_{16}\\F_{12}F_{22}F_{26}\\F_{16}F_{26}F_{66}\end{bmatrix}\begin{Bmatrix}\varepsilon_1^1\\\varepsilon_2^1\\\varepsilon_6^1\end{Bmatrix}+\begin{bmatrix}H_{11}H_{12}H_{16}\\H_{12}H_{22}H_{26}\\H_{16}H_{26}H_{66}\end{bmatrix}\begin{Bmatrix}\varepsilon_1^2\\\varepsilon_2^2\\\varepsilon_6^2\end{Bmatrix} \tag{21}$$

$$\begin{Bmatrix}K_1\\K_2\end{Bmatrix}=\begin{bmatrix}L_{44}&L_{45}\\L_{45}&L_{55}\end{bmatrix}\begin{Bmatrix}\varepsilon_4^3\\\varepsilon_5^3\end{Bmatrix} \tag{22}$$

Where:

$$A_{ij}=\int_{\frac{-h}{2}}^{\frac{h}{2}}Q_{ij}\,dz\quad i=(1,2,4,5,6)$$

$$(B_{ij},D_{ij},E_{ij},F_{ij},H_{ij})=\int_{\frac{-h}{2}}^{\frac{h}{2}}Q_{ij}(z,z^2,z\times m^{-2\left(\frac{z}{H}\right)^2},z^2\times m^{-2\left(\frac{z}{H}\right)^2}\quad,z^2\times m^{-4\left(\frac{z}{H}\right)^2}\quad i=(1,2,6)$$

$$L_{ij} = \int_{-\frac{h}{2}}^{\frac{h}{2}} Q_{ij}\left[1 - 4\left(\frac{z}{H}\right)^2 \ln(m)\right] \times m^{-2\left(\frac{z}{H}\right)^2} dz \quad i = (4,5) \tag{23}$$

5. Navier's solution

The generalized displacements are expanded in a double trigonometric series in terms of unknown parameters in Navier's method. To satisfy the boundary conditions of the problem, the restricted choice of the function in the series is selected. Substitution of the displacement expansion into the governing equations should give a set of algebraic equation among the parameter of the expansion. Assuming the following displacements form to satisfied simply supported boundary conditions [36]:

$$\begin{aligned}
u(x_1,x_2,t) &= \textstyle\sum_{m=1}^{\infty}\sum_{n=1}^{\infty} U_{mn}(t)\cos(\alpha x_1)\sin(\beta x_2)\\
v(x_1,x_2,t) &= \textstyle\sum_{m=1}^{\infty}\sum_{n=1}^{\infty} V_{mn}(t)\sin(\alpha x_1)\cos(\beta x_2)\\
w(x_1,x_2,t) &= \textstyle\sum_{m=1}^{\infty}\sum_{n=1}^{\infty} W_{mn}(t)\sin(\alpha x_1)\sin(\beta x_2)\\
\theta_1(x_1,x_2,t) &= \textstyle\sum_{m=1}^{\infty}\sum_{n=1}^{\infty} \theta_{1mn}(t)\cos(\alpha x_1)\sin(\beta x_2)\\
\theta_2(x_1,x_2,t) &= \textstyle\sum_{m=1}^{\infty}\sum_{n=1}^{\infty} \theta_{2mn}(t)\sin(\alpha x_1)\cos(\beta x_2)
\end{aligned} \tag{24}$$

Where: $\alpha = \frac{m\pi}{a}$, $\beta = \frac{n\pi}{b}$, $(U_{mn}, V_{mn}, W_{mn}, \theta_{1mn}, \theta_{2mn})$, are arbitrary constants.

The Navier solution exists if the following stiffness are zero:

$$A_{16} = B_{16} = D_{16} = E_{16} = F_{16} = H_{16} = A_{26} = B_{26} = D_{26} = E_{26} = F_{26} = H_{26} = A_{45} = J_{45} = L_{45} = 0$$

The equations of motion (16) can be expressed in terms of displacements by substituting Eqs. (19)-(22) and Eq. (24), the following eignvalue equation is obtained:

$$\begin{bmatrix} c_{11} & c_{12} & c_{13} & c_{14} & c_{15}\\ c_{21} & c_{22} & c_{23} & c_{24} & c_{25}\\ c_{31} & c_{32} & c33 - \alpha^2 N_{x1}^T - \beta^2 N_{x2}^T - \alpha\beta N_{x1x2}^T & c_{34} & c_{35}\\ c_{41} & c_{42} & c_{43} & c_{44} & c_{45}\\ c_{51} & c_{52} & c_{53} & c_{54} & c_{55} \end{bmatrix} \begin{Bmatrix} U_{mn}\\ V_{mn}\\ W_{mn}\\ \theta_{1mn}\\ \theta_{2mn} \end{Bmatrix} = 0 \tag{25}$$

Where: C_{ij} is the stiffness element given in appendix.

6. Results and discussion

Thermal buckling of cross ply laminated shallow spherical shells are analyzed by solving equations of motion derived based on Mantari and Reddy displacement fields for first time, using Matlab R2014a programming, material properties used for all figures are:

α_0=1, α_1=0.015*α_0; α_2=1*α_0;To=0; E1=15; E2=1; E3=E2; ν_{12}=0.3; ν_{13}=0; ν_{23}=0.49; GG12=0.5; GG13=0.5; GG23=0.3356, $\bar{T} = \alpha_0 \times T_{cr}$=normalized critical temperature.

First theory is based on a displacement field in which the displacements of the middle surface are expanded as a combination of exponential and polynomial functions of the thickness coordinate (Mantari displacement field), while second theory is based on a displacement field in

Table 1. Normalized critical temperatures of 2- cross-ply laminated shallow shells (a/b =1, m=n=1 for all cases (except when it is written)

	$\bar{T}$		
	References		
	Present work (Mantari function)	Present work (Reddy function)	[29]
Shallowness ratio		a/H=5	
a/R=.1	0.135336	0.118945	0.127158
a/R=.2	0.136654	0.120973	0.133660
a/R=.4	0.144875	0.129103	0.143169
	a/H=10		
a/R=.1	0.046328	0.039156	0.038106
a/R=.2	0.048249	0.041686	0.042379
a/R=.4	0.057759	0.051813	0.056674
	a/H=20		
a/R=.1	0.013225	0.011254	0.012894
a/R=.2	0.015591	0.013969	0.019644
a/R=.4	0.026019	0.024827	0.032534

Table 2. Normalized critical temperatures of 3- cross-ply laminated shallow shells (a/b =1, m=n=1 for all cases (except when it is written)

	$\bar{T}$		
	References		
	Present work (Mantari function)	Present work (Reddy function)	[29]
Shallowness ratio		a/H=5	
a/R=.1	0.146703 m=n=1	0.146604 m=n=1	0.178609
a/R=.2	0.149562 m=n=1	0.148555 m=n=1	0.181867
a/R=.4	0.160996 m=n=1	0.156382 m=n=1	0.194406
	a/H=10		
a/R=.1	0.061855 m=n=1	0.0618584 m=n=1	0.078796
a/R=.2	0.064713 m=n=1	0.064279 m=n=1	0.082481
a/R=.4	0.074073 m=1,n=2	0.073210 m=1,n=2	0.097118
	a/H=20		
a/R=.1	0.019605 m=n=1	0.019555 m=n=1	0.026601
a/R=.2	0.022048 m=1,n=2	0.021977, m=1,n=2	0.032921
a/R=.4	0.028094 m=1,n=2	0.027774 m=1, n=2	0.047090

Table 3. Normalized critical temperatures of (2 and 3) layer cross-ply laminated composite shallow shells (a/b =1, a/R1=b/R2=0.5, m=n=1 for all cases (except when it is written)

$\bar{T}$			
No. of layers=2			
	References		
Thickness ratio	Present work (Mantari function)	Present work (Reddy function)	[29]
5	0.1517784	0.135219	0.1505
10	0.065349	0.059415	0.06863
20	0.034082	0.032972	0.03927
No. of layers=3			
5	0.192131	0.162276	0.1942
10	0.089364	0.077210	0.09874
20	0.042916	0.032122 m=1,n=2	0.04986

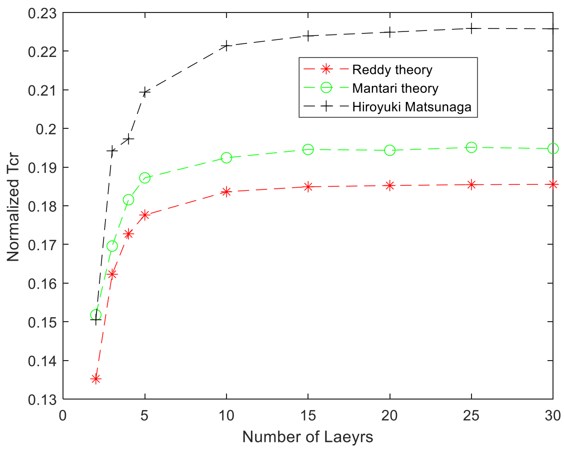

Figure 2. Normalized critical temperatures $\bar{T}$ of cross-ply laminated composite shallow shells (a/b=1, a/H=5, a/R=0.5) for different theories and no. of layers

which the displacements of the middle surface are expanded as a polynomial functions of the thickness coordinate (Reddy displacement field) are compared with third shear deformation theory which based on displacement components may be expanded into power series of the thickness coordinate [29] and the transverse displacement is assumed to be constant through the shell thickness for these three shear deformation shell theories. Normalized critical temperatures obtained from three different theories are shown in Tables 1-2 and Fig. 2, they are decrease when thickness ratio increase and increase when shallowness ratio increase so it has same behavior, for thick shell, Reddy function gives under predict critical temperature while for thinner shell results from these theories are close to each other, also when changing shell curvature differ for thick shell and closer for thinner shell.

Effect of number of layers on thermal buckling behavior is shown in Table 3, which is a direct relation as expected, except that for second theory, the mode of minimum thermal buckling

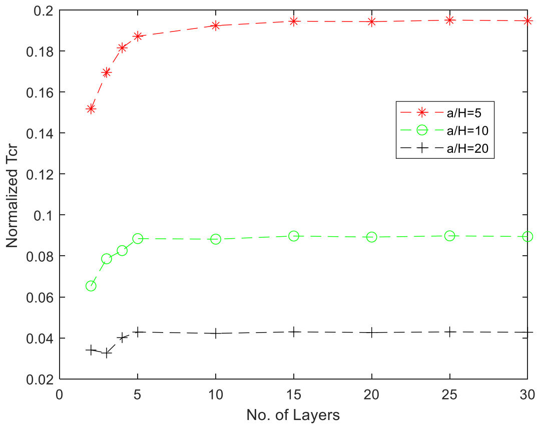

Figure 3. Normalized critical temperatures $\bar{T}$ of cross-ply laminated composite shallow shells (a/b=1, a/R=0.5) for different no. of layers and thickness ratio, based on Mantari function

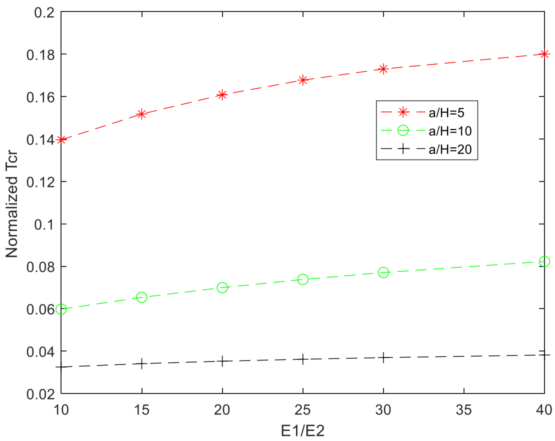

Figure 4. Normalized critical temperatures $\bar{T}$ of [0/90] cross-ply laminated shallow shells (a/b=1, a/R=0.5) for different orthotropy and thickness ratio based on Mantari function

changes for three layers with thickness ratio=20, and they are closed to each other but Reddy theory is under predicted compared with other two and is closed to Mantari function, but when increasing number of layers critical temperature will increase until five layers and then it tends to be constant as shown in Fig. 3. while increasing orthotropic ratio that cause increasing shell stiffness results as shown in Fig. 4.

7. Conclusions

In present work different shell theories are investigated to obtain critical temperatures of simply supported shell, (Mantari displacement field) and (Reddy displacement field) are compared with third shear deformation theory (Matsunaga). Normalized critical temperatures obtained from three different theories with changing design parameters have same behavior except that for second theory, the mode of minimum thermal buckling sometimes changed, and they are closed to each other, for thick shell, Reddy function gives under predict critical temperature while for thinner shell results from these theories are close to each other, also when changing shell curvature differ for thick shell and closer for thinner shell.

References

1. Akbaş, Ş.D. (2022). Thermal post-buckling analysis of a laminated composite beam. Structural Engineering and Mechanics, 337-346. https://doi.org/10.12989/sem.2018.67.4.337.
2. She, G.L., Ren, Y.R., Xiao, W.S., Liu, H.B. (2018). Study on thermal buckling and post-buckling behaviors of FGM tubes resting on elastic foundations. Structural Engineering and Mechanics, 66(6), 729-736. https://doi.org/10.12989/sem.2018.66.6.729.
3. Noor, A.K., Burton, W.S. (1992). Three-dimensional solutions for the thermal buckling and sensitivity derivatives of temperature-sensitive multilayered angle-ply plates. Journal of Applied Mechanics, 59(4), 848-856. https://doi.org/10.1115/1.2894052.
4. Sadiq, I. A. (2019). Thermal buckling of angle-ply laminated plates using new displacement function. Journal of Engineering, 25(12), 96-113. https://doi.org/10.31026/j.eng.2019.12.08.
5. Majeed, W.I., Sadiq, I.A. (2022). Thermal buckling of laminated plates using modified Mantari function. Journal of Mechanical Engineering, 19(3), 205-20.
6. Majeed, W.I., Sadiq, I.A. (2022). Thermal buckling and stability of laminated plates under non uniform temperature distribution. Steel and Composite Structures, 14(4), 503-511. https://doi.org/10.12989/scs.2023.47.4.503.
7. Cetkovic, M. (2016). Thermal buckling of laminated composite plates using layerwise displacement model. Composite Structures, 142, 238-253. https://doi.org/10.1016/j.compstruct.2016.01.082.
8. Yuksel, Y.Z., Akbas, S.D. (2021). Hygrothermal stress analysis of laminated composite porous plates. Structural Engineering and Mechanics, 80(1), 1-13. https://doi.org/10.12989/sem.2021.80.1.001.
9. Abualnour, M., Chikh, A., Hebali, H., Kaci, A., Tounsi, A., Bousahla, A.A., Tounsi, A. (2019). Thermomechanical analysis of antisymmetric laminated reinforced composite plates using a new four variable trigonometric refined plate theory. Computers and Concrete, 24(6), 489-498. https://doi.org/10.12989/cac.2019.24.6.489.
10. Belbachir, N., Bourada, M., Draiche, K., Tounsi, A., Bourada, F., Bousahla, A.A., Mahmoud, S.R. (2020). Thermal flexural analysis of anti-symmetric cross-ply laminated plates using a four variable refined theory. Smart Structures and Systems, 25(4), 409-422. https://doi.org/10.12989/sss.2020.25.4.409.
11. Hashim, H.A., Sadiq, I.A. (2023). Uniform and non-uniform thermal buckling analysis of laminated plates using five-variable refined theory. AIP Conference Proceedings, 2651(1), 050009. https://doi.org/10.1063/5.0106917.
12. Abdul-Majeed, W.R., Jweeg, M.J., Jameel, A.N. (2011). Thermal buckling of rectangular plates with different temperature distribution using strain energy method. Journal of Engineering, 17(05), 1047-1065. https://doi.org/10.31026/j.eng.2011.05.02.
13. Jameel, A.N., Sadiq, I.A., Nsaif, H.I. (2012). Buckling analysis of composite plates under thermal and mechanical loading. Journal of Engineering, 18(12), 1365-1389. https://doi.org/10.31026/j.eng.2012.12.06.
14. Zohra, A., Rabia, B., Tahar, H.D. (2023). Critical thermal buckling analysis of porous FGP sandwich plates under various boundary conditions. Structural Engineering and Mechanics, 87(1), 29-46. https://doi.org/10.12989/sem.2023.87.1.029.
15. Tahir, S.I., Chikh, A., Tounsi, A., Al-Osta, M.A., Al-Dulaijan, S.U., Al-Zahrani, M.M. (2021). Wave propagation analysis of a ceramic-metal functionally graded sandwich plate with different porosity distributions in a hygro-thermal environment. Composite Structures, 269, 114030. https://doi.org/10.1016/j.compstruct.2021.114030.
16. Shiau, L.C., Kuo, S.Y., Chen, C.Y. (2010). Thermal buckling behavior of composite laminated plates.

Composite Structures, 92(2), 508-514. https://doi.org/10.1016/j.compstruct.2009.08.035.
17. Yang, F., Xie, W. (2022). Thermal buckling behavior of Bouligand inspired laminated composite plates. Journal of Composite Materials, 56(26), 3939-3947. https://doi.org/10.1177/00219983221125905.
18. Cho, J.R. (2023). Numerical study on the thermal buckling of functionally graded sandwich plates. Journal of Mechanical Science and Technology, 37(4), 1913-1922. https://doi.org/10.1007/s12206-023-0328-6.
19. Cho, J.R. (2024). Thermal buckling and postbuckling analysis of cracked FG-GPL RC plates using a phase-field crack model. Applied Sciences, 14(19), 8794. https://doi.org/10.3390/app14198794.
20. Lee, J.J., Oh, I.K., Lee, I., Yeom, C.H. (2002). Thermal post-buckling behavior of patched laminated panels under uniform and non-uniform temperature distributions. Composite Structures, 55(2), 137-145. https://doi.org/10.1016/S0263-8223(01)00139-8.
21. Panda, S.K., Singh, B.N. (2009). Thermal post-buckling behaviour of laminated composite cylindrical/hyperboloid shallow shell panel using nonlinear finite element method. Composite Structures, 91(3), 366-374. https://doi.org/10.1016/j.compstruct.2009.06.004.
22. Katariya, P.V., Panda, S.K. (2016). Thermal buckling and vibration analysis of laminated composite curved shell panel. Aircraft Engineering and Aerospace Technology, 88(1), 97-107. https://doi.org/10.1108/AEAT-11-2013-0202.
23. Narayan, D.A., Ganapathi, M., Pradyumna, B., Haboussi, M. (2019). Investigation of thermo-elastic buckling of variable stiffness laminated composite shells using finite element approach based on higher-order theory. Composite Structures, 211, 24-40. https://doi.org/10.1016/j.compstruct.2018.12.012.
24. Trabelsi, S., Zghal, S., Dammak, F. (2020). Thermo-elastic buckling and post-buckling analysis of functionally graded thin plate and shell structures. Journal of the Brazilian Society of Mechanical Sciences and Engineering, 42(5), 233. https://doi.org/10.1007/s40430-020-02314-5.
25. Cho, J.R. (2022). Thermal buckling analysis of metal-ceramic functionally graded plates by natural element method. Structural Engineering and Mechanics, 84(6), 723-731. https://doi.org/10.12989/sem.2022.84.6.723.
26. Katariya, P.V., Panda, S.K. (2022). Numerical analysis of thermal post-buckling strength of laminated skew sandwich composite shell panel structure including stretching effect. Steel and Composite Structures, 279-288. https://doi.org/10.12989/scs.2020.34.2.279.
27. Azzara, R., Carrera, E., Filippi, M., Pagani, A. (2023). Vibration analysis of thermally loaded isotropic and composite beam and plate structures. Journal of Thermal Stresses, 46(5), 369-386. https://doi.org/10.1080/01495739.2023.2188399.
28. Sahoo, B., Mehar, K., Sahoo, B., Sharma, N., Panda, S.K. (2021). Thermal frequency analysis of FG sandwich structure under variable temperature loading. Structural Engineering and Mechanics, 77(1), 57-74. https://doi.org/10.12989/sem.2021.77.1.057.
29. Matsunaga, H. (2007). Thermal buckling of cross-ply laminated composite shallow shells according to a global higher-order deformation theory. Composite Structures, 81(2), 210-221. https://doi.org/10.1016/j.compstruct.2006.08.008.
30. Topal, U.M.U.T., Uzman, Ü. (2009). Thermal buckling load optimization of angle-ply laminated cylindrical shells. Materials & Design, 30(3), 532-536. https://doi.org/10.1016/j.matdes.2008.05.052.
31. Vaikunthbhai, K.P. (2014). Free vibration and buckling behaviour of laminated composite panel under thermal and mechanical loading. M.Sc. Dissertation, National Institute of Technology Rourkela, Odisha, India.
32. Madeh, A.R., Majeed, W.I. (2021). Effect of boundary conditions on thermal buckling of laminated composite shallow shell. Materials Today: Proceedings, 42, 2397-2404. https://doi.org/10.1016/j.matpr.2020.12.501.
33. Taih, F.H., Majeed, W.I. (2024). Thermal buckling analysis of composite laminated shells using higher order shear deformation theory. International Review on Modelling & Simulations, 17(4), 256. https://doi.org/10.15866/iremos.v17i4.24972.
34. Xu, J.Q., She, G.L. (2023). Thermal post-buckling of graphene platelet reinforced metal foams doubly curved shells with geometric imperfection. Structural Engineering and Mechanics, 87(1), 85-94.

https://doi.org/10.12989/sem.2023.87.1.085.

35. Mantari, J.L., Oktem, A.S., Soares, C.G. (2011). Static and dynamic analysis of laminated composite and sandwich plates and shells by using a new higher-order shear deformation theory. Composite Structures, 94(1), 37-49. https://doi.org/10.1016/j.compstruct.2011.07.020.
36. Reddy, J.N. (2004), Mechanics of laminated composite plates and shells: theory and analysis. CRC Press, Florida, USA

Appendix

First HSDT stiffness elements of C_{ij} are:

$$C_{11} = -A_{11}\alpha^2 - A_{66}\beta^2$$
$$C_{12} = C_{21} = -A_{12}\alpha\,\beta - A_{66}\alpha\,\beta$$
$$C_{13} = C_{31} = B_{11}\alpha^3 + B_{12}\alpha\beta^2 + 2B_{66}\alpha\beta^2 + A_{11}\frac{\alpha}{R_1} + A_{12}\frac{\alpha}{R_2}$$
$$C_{14} = C_{41} = -E_{11}\alpha^2 - E_{66}\beta^2$$
$$C_{15} = C_{51} = -E_{12}\alpha\,\beta - E_{66}\alpha\,\beta$$
$$C_{22} = -A_{22}\beta^2 - A_{66}\alpha^2$$
$$C_{23} = C_{32} = B_{12}\alpha^2\beta + B_{22}\beta^3 + 2B_{66}\alpha^2\beta + A_{21}\frac{\beta}{R_1} + A_{22}\frac{\beta}{R_2}$$
$$C_{24} = C_{42} = -E_{12}\alpha\,\beta - E_{66}\alpha\,\beta$$
$$C_{25} = C_{52} = -E_{22}\beta^2 - E_{66}\alpha^2$$
$$C_{33} = -D_{11}\alpha^4 - 2D_{12}\alpha^2\beta^2 - D_{22}\beta^4 - 4D_{66}\alpha^2\beta^2 - 2\frac{\beta^2}{R_1}B_{12} - 2\frac{\beta^2}{R_2}B_{22} - 2\frac{\alpha^2}{R_2}B_{12} - 2\frac{\alpha^2}{R_1}B_{11} - \frac{1}{R_2{}^2}A_{22} - 2\frac{1}{R_1R_2}A_{21} - \frac{1}{R_1{}^2}A_{11}$$
$$C_{34} = C_{43} = E_{11}\frac{\alpha}{R_1} + E_{12}\frac{\alpha}{R_2} + F_{12}\alpha\beta^2 + F_{11}\alpha^3 + 2F_{66}\alpha\,\beta^2$$
$$C_{35} = C_{53} = E_{12}\frac{\beta}{R_1} + E_{22}\frac{\beta}{R_2} + F_{12}\alpha^2\beta + F_{22}\beta^3 + 2F_{66}\alpha^2\beta$$
$$C_{44} = -H_{11}\alpha^2 - H_{66}\beta^2 - L_{55}$$
$$C_{45} = C_{54} = -H_{12}\,\alpha\,\beta - H_{66}\,\alpha\,\beta$$
$$C_{55} = -H_{22}\beta^2 - H_{66}\alpha^2 - L_{44}$$

Second HSDT stiffness elements of C_{ij} are:

C(1,1)=-A11*(α^2)-((8*E11* α^2)/(3*R1*H^2))-A66*(β^2)-((8*E66* β^2)/(3*R1*H^2))-((A55)/(R1^2))+((8*D55)/((R1^2)*(H^2)))-(16*F55)/((R1^2)*(H^4))-(16*H66* β^2)/(9*(R1^2)*(H^4))-(16*H11*A^2)/(9*(R1^2)*(H^4))

C(1,2)=-A12* α* β-((4*E12* α* β)/(3*R2*H^2))-((4*E12* α* β)/(3*R1*H^2))-A66* α* β-((4*E66* α* β)/(3*R2*H^2))-((4*E66* α* β)/(3*R1*H^2))-(16*H12* α* β)/(9*R1*R2*H^4))-((16*H66* α * β)/(9*R1*R2*H^4));

C(1,3)=((α*A11)/(R1))+((4*E11* α^3)/(3*H^2))+((α*A12)/(R2))+((4*E12* α* β^2)/(3*H^2))+(8*E66* α* β^2)/(3*H^2))+((α*A55)/(R1))+((32*H66* α* β^2)/(9*R1*H^4))-((8*D55* α)/(R1*H^2))+((16*F55* α)/(R1*H^4))+((4*E11* α)/(3*(R1^2)*H^2))+((16*H11* α ^3)/(9*R1*H^4))+((4*E12* α)/(3*R1*R2*H^2))+((16*H12* α * β ^2)/(9*R1*H^4))

C(1,4)=-(B11* α^2)+((4*E11* α^2)/(3*H^2))-(B66* β^2)+((4*E66* β^2)/(3*H^2))+(A55/(R1))-(8*D55/(R1*H^2))+(16*F55/(R1*H^4))-((4*F11* α^2)/(3*R1*H^2))+((16*H11* α^2)/(9*R1*H^4))-((4*F66* β^2)/(3*R1*H^2))+((16*H66* β ^2)/(9*R1*H^4))

C(1,5)=- α* β*(B12+B66)+((4*E12* α* β)/(3*H^2))+((4*E66* α* β)/(3*H^2))-
((4*F12* α* β)/(3*R1*H^2))+((16*H12* α* β)/(9*R1*H^4))-
((4*F66* α* β)/(3*R1*H^2))+((16*H66* α * β)/(9*R1*H^4))

C(2,2)=-(A66* α^2)-(A22* β^2)-(A44/(R2^2))-((8*E66* α^2)/(3*R2*H^2))-
((8*E22* β^2)/(3*R2*H^2))+(8*D44/((R2^2)*(H^2)))-(16*F44/((R2^2)*(H^4)))-((16*H66* α
^2)/(9*(R2^2)*(H^4)))-((16*H22* β ^2)/(9*(R2^2)*(H^4)))

C(2,3)=(8*E66* β* α^2)/(3*H^2))+(A12* β/(R1))+((4*E21* β* α^2)/(3*H^2))+(A22* β/(R2))+((
4*E22* β^3)/(3*H^2))+(A44* β/(R2)))))+((16*H22* β^3)/(9*R2*H^4))-
((8*D44* β)/(R2*H^2))+((16*F44* β)/(R2*H^4))+((32*H66* β* α^2)/(9*R2*H^4))+((4*E21* β)
/(3*R2*R1*H^2))+((16*H21* β * α ^2)/(9*R2*H^4))+((4*E22* β)/(3*(R2^2)*(H^2

C(2,4)=- α* β*B66-(β* α*B21)+((4*E66* β* α)/(3*H^2))+((4*E21* β* α)/(3*H^2))-
((4*F66* β* α)/(3*R2*H^2))+((16*H66* β* α)/(9*R2*H^4))-
((4*F21* β* α)/(3*R2*H^2))+((16*H21* β * α)/(9*R2*H^4))

C(2,5)=-((α^2)*B66)-))-((8*D44)/(R2*H^2))+((16*F44)/(R2*H^4))-
(B22*(β^2))+(A44/(R2))+((4*E66* α^2)/(3*H^2))+((4*E22* β^2)/(3*H^2-
((4*F66* α^2)/(3*R2*H^2))+((16*H66* α^2)/(9*R2*H^4))-
((4*F22* β^2)/(3*R2*H^2))+((16*H22* β ^2)/(9*R2*H^4));

C(3,3)=-(A55* α^2)-(A44* β^2)+((8*D55* α^2)/(H^2))-
((16*F55* α^2)/(H^4))+((8*D44* β^2)/(H^2))-((16*F44* β^2)/(H^4))-
((8*E11* α^2)/(3*R1*H^2))-((16*H11* α^4)/(9*H^4))-((4*E12* α^2)/(3*R1*H^2))-
((8*E12* β^2)/(3*R1*H^2))-((32*H12*(α^2)*(β^2))/(9*H^4))-((8*E22* β^2)/(3*R2*H^2))-
((16*H22* β^4)/(9*H^4))-((64*H66*(β^2)*(α^2))/(9*(H^4)))-(A11/(R1^2))-(2*A12/(R1*R2))-
(A22/(R2^2))-((4*E12* α ^2)/(3*R2*H^2));

C(3,4)=- α*A55+(α*B11/(R1))+((8* α*D55)/(H^2))-
((16* α*F55)/(H^4))+((4*(α^3)*F11)/(3*H^2))-
((16*(α^3)*H11)/(9*H^4))+((4*(α* β^2)*F12)/(3*H^2))-
((16*(α* β^2)*H12)/(9*H^4))+((8*(α* β^2)*F66)/(3*H^2))-((32*(α* β^2)*H66)/(9*H^4))-
((4* α *E11)/(3*R1*H^2))+(α *B12/(R2))-((4* α *E12)/(3*R2*H^2));

C(3,5)=-B*A44+(8* β*D44/(H^2))-((16* β*F44)/(H^4))+((4*(α^2)* β*F12)/(3*H^2))-
((16*(α^2)* β*H12)/(9*H^4))+((4*(β^3)*F22)/(3*H^2))-
((16*(β^3)*H22)/(9*H^4))+((8*(α^2)* β*F66)/(3*H^2))-
((32*(α^2)* β*H66)/(9*H^4))+(β*B12/(R1))-((4* β*E12)/(3*R1*H^2))+(B22* β/(R2))-((4* β
*E22)/(3*R2*H^2));

C(4,4)=-D11*(α^2)+((8*(α^2)*F11)/(3*H^2))-((16*(α^2)*H11)/(9*H^4))-
D66*(β^2)+((8*(β^2)*F66)/(3*H^2))-A55-((16*(β^2)*H66)/(9*H^4))+(8*D55/(H^2))-
(16*F55/(H^4));

C(4,5)=-D12*(α* β)+((8*(α* β)*F12)/(3*H^2))-((16*(α* β)*H12)/(9*H^4))-D66*(β* α)+((8*(β * α)*F66)/(3*H^2))-((16*(β * α)*H66)/(9*H^4));

C(5,5)=-D66*(α^2)+((8*(α^2)*F66)/(3*H^2))-((16*(α^2)*H66)/(9*H^4))-D22*(β^2)+((8*(β^2)*F22)/(3*H^2))-A44-((16*(β^2)*H22)/(9*H^4))+(8*D44/(H^2))-(16*F44/(H^4))